Acta Cryst. (1981). A**37**, 826–837

X-ray Study of the Charge Distribution in MgF_2

BY J. P. VIDAL

Laboratoire de Cristallographie (*LA* 233), *Place E. Bataillon, Université des Sciences et Techniques du Languedoc*, 34060 *Montpellier CEDEX, France*

G. VIDAL-VALAT AND M. GALTIER

Laboratoire d'Infrarouge (*LA* 233), *Place E. Bataillon, USTL*, 34060 *Montpellier CEDEX, France*

AND K. KURKI-SUONIO

Department of Physics, University of Helsinki, Siltavuorenpenger 20 *D, SF*-00170 *Helsinki* 17, *Finland*

(*Received* 9 *July* 1980; *accepted* 21 *April* 1981)

Abstract

X-ray structure factors of MgF_2 were derived from accurate measurement of single-crystal diffraction intensities. The crystal charge density was analyzed in terms of multipole expansions centered at the ionic sites. Separation of electronic and dynamic deformations was effected by using, in the difference series calculations, anisotropic Debye–Waller factors obtained in the neutron diffraction study of Vidal-Valat, Vidal, Zeyen & Kurki-Suonio [*Acta Cryst.* (1979), B**35**, 1584–1590]. The charge density was found to be composed of well defined local Mg^{2+} ions and slightly enlarged and more diffuse F^- ions with 0·50 electrons distributed more widely in the unit cell. Nonspherical deformations of electronic origin were found significant up to fourth order, with the exception of the vanishing dipole moment of fluorine. These deformations emphasize the ionic nature of the crystal by violating the symmetry of the immediate surroundings and by decreasing the charge density in all of the octahedral bonding directions of Mg^{2+} down to typical ionic values.

0567-7394/81/060826-12$01.00

Introduction

The peculiar anisotropic optical properties combined with a relatively simple structure have created an interest in magnesium fluoride, *e.g.* because of its possible use in ultraviolet spectroscopy as a reflective coating for mirrors and gratings. In a range below 1240 Å it acts as a highly efficient polarizer. Consequently, it has been subject to a series of investigations, both experimental and theoretical, in order to measure its characteristics and to trace the origin of the observable properties. These studies involve measurements of optical constants from reflexion and absorption spectra (Williams, MacRae & Arakawa, 1967; Rabe, Sonntag, Sagawa & Haensel, 1972; Thomas, Stephan, Lemonnier, Nisar & Robin, 1973) and from energy losses of fast electrons (Gout, Lahaye & Perrier, 1967; Venghaus, 1971), studies of the electronic structure by photoelectron spectroscopy (Poole, Szajhan, Leckey, Jenkin & Liesegang, 1975) and related theoretical band structure calculations (Jouanin & Gout, 1972; Jouanin, Albert & Gout, 1976). Measurements of the phonon dispersion curves have been made by inelastic neutron scattering (Almairac, 1975) and by infrared and Raman spectroscopy (Barker, 1964; Porto, Fleury & Damen, 1967). Extensive lattice dynamical model calculations have been made to explain and interpret such measurements (Mishra, Padhy & Mohanty, 1977; Matsumoto, Urabe & Kanamori, 1978) and to relate the lattice dynamical properties to the electronic ones (Almairac & Benoit, 1974). In many of these studies a strongly ionic character for MgF_2 has been assumed and found to yield a good agreement between theory and observations. Also, the more direct experimental measures of ionicity obtained in these studies indicate consistently almost complete ionization into Mg^{2+} and F^- of the atoms in the crystal and an ionic nature of the crystal comparable to that of the alkaline halides.

The only charge density study of MgF_2 so far is that made by Niederauer & Göttlicher (1970) at room temperature. They observed some charge density bridges between magnesium and its six fluorine neighbors as if there were a covalent bonding contribution. They also reported isotropic thermal vibrations of both ions.

In order to get a more detailed and accurate picture of the information available by diffraction methods on the nature of the MgF_2 crystal a combined neutron and X-ray diffraction investigation was undertaken. Results of the neutron diffraction study have already been published (Vidal-Valat, Vidal, Zeyen & Kurki-Suonio, 1979). Anisotropic thermal parameters were found in good agreement with theoretical values calculated on the basis of the lattice dynamical model of Almairac & Benoit (1974). In this paper the X-ray diffraction measurements and their analysis are reported. The necessary details of the lattice dynamical calculations are attached as an Appendix.

Experimental

Single crystals of MgF_2 were grown in the Laboratoire de Physique Moléculaire of the Université des Sciences et Techniques du Languedoc, Montpellier. A preliminary X-ray study showed strong extinction in this crystal. The crystal was quenched in order to eliminate primary extinction, *cf.* Vidal-Valat *et al.* (1979). As a result about 30% increase of intensity was observed in the most extinguished reflections. Several specimens were cleaved from a large crystal. The crystal displaying the smallest extinction effect was chosen for the ordinary study.

Basic crystallographic data on MgF_2 and on the specimen are listed in Table 1. The cell parameters were determined by least squares on the basis of the X-ray diffraction pattern. They agree accurately with the values obtained in the neutron study (Vidal-Valat *et al.*, 1979). For the position parameter of fluorine the value found in that work is adopted.

Relative intensities of 97 independent reflections up to 0·85 $Å^{-1}$ in $\sin\theta/\lambda$ were collected at 300 K in one whole octant on an automatic three-circle Enraf–Nonius CAD-3 diffractometer with Mo $K\alpha$ radiation. The controlled symmetry-related reflections displayed no more than a 2% discrepancy in intensities. The technical performance and geometrical information of the diffractometer have been reported by Vidal-Valat, Vidal & Kurki-Suonio (1978).

Background was measured for half the scan time at each end of the scan. The receiving aperture size on the detector and the scan width were programmed and varied with Bragg angle in such a way that the selected scan width made the recorded background a minimum, *cf.* Vidal-Valat, Vidal & Kurki-Suonio (1975).

The overall dead-time of the counting circuit was 4 μs. At the maximum counting rate (less than 1200 counts s^{-1}) occurring in the measurements this cor-

Table 1. *Crystallographic data*

Space group	$P4_2/mnm$
Crystal dimensions	0·15 × 0·25 × 0·28 mm
Cell parameters	$a = b = 4{\cdot}628$ (5) Å
	$c = 3{\cdot}045$ (3)
Atomic positions	Mg^{2+} (0,0,0); $(\frac{1}{2},\frac{1}{2},\frac{1}{2})$
	F^- ± $(x,x,0)$; $(\frac{1}{2},\frac{1}{2},\frac{1}{2})$ ± $(x,-x,0)$,
	$x = 0{\cdot}3032$ (2)
Mg–F distance	1·984 (1) Å
Linear absorption coefficient (Mo $K\alpha$)	0·695 mm^{-1}
Anomalous scattering coefficients (for Mo $K\alpha$) (Cromer & Liberman, 1970)	Mg^{2+} $f' = 0{\cdot}042$
	$f'' = 0{\cdot}036$
	F^- $f' = 0{\cdot}014$
	$f'' = 0{\cdot}010$

responds to a dead-time correction of less than 1%. Multiple scattering was eliminated by independent setting of crystallographic and diffractometer axes.

Lorentz and polarization corrections, the absorption correction of Busing & Levy (1957) and the anomalous dispersion corrections of Cromer & Liberman (1970) were applied to the intensities.

To correct for the residual extinction effects, refinements with different extinction models were applied to the entire set of experimental intensities using the *LINEX* program of Becker & Coppens (1975). In these refinements the anisotropic Debye–Waller factors and the bond length were kept fixed. The experimental values obtained in the neutron diffraction study of Vidal-Valat *et al.* (1979) were adopted. Further support for the values of Debye–Waller factors was obtained by a lattice dynamical calculation reported in the Appendix. The scale was refined together with the extinction parameters. All different combinations of extinction models were used: isotropic and anisotropic, mosaic-spread and particle-size type of extinction, with and without primary extinction. The results were very similar to those obtained in the case of neutron diffraction. Isotropic mosaic-spread extinction gave a lower R factor (0·012) than the particle-size extinction (0·014) and no significant improvement was obtained by any of the more sophisticated models. Therefore the extinction corrections were made according to the isotropic mosaic-spread extinction model.

As a further check of the relevance of the Debye–Waller factors we derived their values from a fit to the X-ray data up to different cut-off values of $\sin\theta/\lambda$ from 0·4 to 0·85 Å^{-1}. To eliminate the dependence on the scale, the scale factor was kept fixed.

The parameters were found to reach certain asymptotic values, within experimental accuracy, given in Table 2 together with the neutron values and the lattice dynamical ones. There is a good agreement between all the values. The stability of the X-ray values against the cut-off at large $\sin\theta/\lambda$ shows that X-ray data do not indicate deviations of the ionic form factors from the theoretical ones beyond $\sin\theta/\lambda = 0{\cdot}6$ Å^{-1}.

Table 2. *Atomic mean-square displacements* (Å^2) *of* MgF_2

		X-ray values	Neutron values	Lattice dynamical values
Mg^{2+}	$u_{11} = u_{22}$	0·0054 (3)	0·0053 (3)	0·0066
	u_{33}	0·0039 (3)	0·0036 (3)	0·0046
	u_{12}	−0·0005 (3)	−0·0004 (2)	−0·0006
F^-	$u_{11} = u_{22}$	0·0084 (3)	0·0087 (2)	0·0065
	u_{33}	0·0069 (4)	0·0062 (2)	0·0068
	u_{12}	−0·0033 (3)	−0·0034 (2)	−0·0034
R		0·011	0·010	
R_w		0·014	0·014	

The experimental structure factors F_o on an absolute scale corrected for isotropic mosaic-spread extinction and for anomalous dispersion, as obtained from the refinement with fixed neutron temperature parameters, were adopted as the starting values of the charge density analysis. The structure factors beyond 0·6 Å^{-1} in $\sin\theta/\lambda$ were omitted in this analysis since, as stated, they do not contain any further information on the electronic deformations. These values are given in Table 3.

The uncertainties ΔF are the standard errors (of the mean) for each group of three experimental determinations. Thus, they give estimates of random errors but do not attempt to include systematic errors.

The principles of the analysis

The analysis is based on representation of the crystal charge density as a site-symmetric multipole expansion (Kurki-Suonio, 1977):

$$\rho(\mathbf{r}) = \sum_{lmp} \rho_{lmp}(r)\, \mathscr{Y}_{lmp}(\theta,\varphi) \qquad (1)$$

Table 3. *Calculated and observed structure factors of* MgF_2 *with relative errors and extinction coefficients*

H	K	L	B	F_c	F_o	$\pm\Delta F_o/F_o$	y
1	1	0	0.306	21.522	22.014	0.015	0.58
1	0	1	0.393	8.348	8.749	0.019	0.95
2	0	0	0.432	-3.349	-3.620	0.010	0.99
1	1	1	0.448	-22.412	-21.681	0.015	0.75
2	1	0	0.483	13.911	14.193	0.002	0.85
2	1	1	0.584	20.039	19.546	0.003	0.83
2	2	0	0.611	25.757	25.670	0.010	0.68
0	0	2	0.657	31.609	31.997	0.007	0.69
3	1	0	0.683	8.871	9.168	0.009	0.95
2	2	1	0.694	-5.989	-5.680	0.001	0.99
1	1	2	0.724	14.493	14.587	0.015	0.92
3	0	1	0.727	25.713	25.543	0.010	0.79
3	1	1	0.758	7.366	7.384	0.020	0.9[illegible]
3	2	0	0.779	-4.963	-5.112	0.020	0.99
2	0	2	0.786	0.931	0.990	0.020	1.00
2	1	2	0.815	7.921	7.867	0.010	0.98
3	2	1	0.845	2.597	2.449	0.020	1.00
4	0	0	0.864	13.573	13.851	0.010	0.92
4	1	0	0.891	-10.629	-10.881	0.007	0.95
2	2	2	0.897	17.588	17.303	0.015	0.91
3	3	0	0.917	17.805	17.954	0.010	0.87
3	1	2	0.948	6.969	6.886	0.020	0.99
4	1	1	0.949	8.671	8.770	0.001	0.98
4	2	0	0.966	7.924	8.210	0.019	0.97
3	3	1	0.974	-2.478	-2.370	0.004	1.00
1	0	3	1.009	5.975	6.313	0.009	0.99
3	2	2	1.019	-3.415	-3.373	0.007	1.00
4	2	1	1.021	5.677	5.717	0.010	0.99
1	1	3	1.031	-8.650	-8.738	0.010	0.98
4	3	0	1.084	4.714	4.948	0.009	0.99
4	0	2	1.086	10.260	10.471	0.001	0.97
2	1	3	1.097	10.593	10.582	0.010	0.97
5	1	0	1.102	10.698	10.937	0.010	0.96
4	1	2	1.107	-7.767	-7.793	0.008	0.99
3	3	2	1.128	13.504	13.205	0.005	0.96
4	3	1	1.129	9.592	9.358	0.010	0.98
5	0	1	1.129	-0.340	-0.323	0.031	1.00
5	1	1	1.150	0.851	0.909	0.022	1.00
2	2	3	1.159	-2.954	-2.961	0.020	1.00
* 5	2	0	1.165	-0.048			
4	2	2	1.168	6.210	6.037	0.005	0.99
3	0	3	1.179	14.034	14.166	0.010	0.96
3	1	3	1.199	3.863	3.891	0.010	1.00

* Unobserved reflection.

centered at the atomic positions. Here, the $\mathscr{Y}_{lmp}$ denote the real spherical harmonics

$$\mathscr{Y}_{lm\pm}(\theta,\varphi) = C_{lm} \sin^m \theta \frac{\mathrm{d}^m P_l(\cos\theta)}{(\mathrm{d}\cos\theta)^m} \begin{cases} \cos m\varphi \\ \sin m\varphi \end{cases}, \quad (2)$$

where $P_l(Z)$ are the Legendre polynomials and the spherical coordinates (θ,φ) refer to local coordinate systems specified separately for each atomic site (Figs. 1,2). Throughout the representation of results in this paper normalization is chosen to yield $\max\{\mathscr{Y}_{lmp}\} = 1$ so that each component ρ_{lmp} given shows directly the contribution of that component to the charge density in the direction where it is largest.

The axes 1,2,3 in Figs. 1 and 2 show the symmetry-adapted coordinate axes for each ion. Magnesium has site symmetry *mmm* corresponding to the index rule $(lmp) = (2\lambda,2\mu,+)$ (Kurki-Suonio, 1977; Kurki-Suonio, Merisalo & Peltonen, 1979) for (1). The symmetry of the fluorine site is *mm*2. With the choice of axes $(1,2,3) = (x,y,z)$ this gives $(lmp) = [l, l-2, (-1)^l]$. Particular attention is paid to the spherical term $\rho_0(=\rho_{00+})$. The average spherical radial densities $4\pi r^2 \rho_0(r)$ and the spherical electron counts

$$Z(r;\mathbf{r}_0) = \int_0^r 4\pi r^2 \rho_0(r,\mathbf{r}_0)\,\mathrm{d}r \quad (3)$$

are calculated at both atomic sites $\mathbf{r}_0$ with the series

$$\rho_0(r,\mathbf{r}_0) = \frac{1}{V}\sum_j F_j \frac{\sin 2\pi S_j r}{2\pi S_j r} \exp(-2\pi i \mathbf{S}_j.\mathbf{r}_0) \quad (4)$$

with j running through all reciprocal-lattice points $\mathbf{S}_j$.

To evaluate the residual terms these quantities were calculated also for a crystal with Gaussian atoms, fitted to the theoretical atomic scattering factors asymptotically at large $\sin\theta/\lambda$. The respective difference series obtained from (4) were added to the Gaussian analytic results to yield the theoretical and experimental values, respectively. The results are shown in Figs. 3 and 4.

The primary discussion of the significance of the different nonspherical components and the subsequent conclusions concerning the atomic deformations are based on the reciprocal-space expansion

$$f(S;\mathbf{r}_0,R) = \sum f_{lmp}(S;\mathbf{r}_0,R)\mathscr{Y}_{lmp}(\theta_s,\varphi_s), \quad (5)$$

which represents the scattering factor of a sphere of radius R and center at $\mathbf{r}_0$ partitioned from the crystal charge density (1). The radial scattering amplitudes of this expansion can be calculated from the series

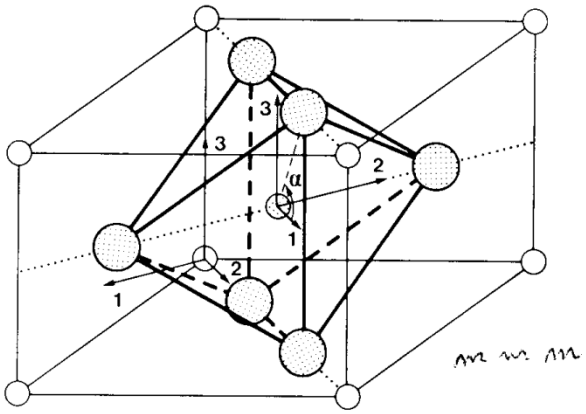

Fig. 1. The surroundings and the local coordinate axes of Mg^{2+} in MgF_2.

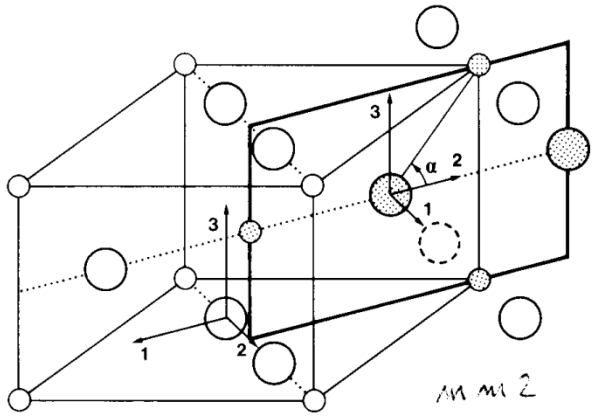

Fig. 2. The surroundings and the local coordinate axes of F^- in MgF_2.

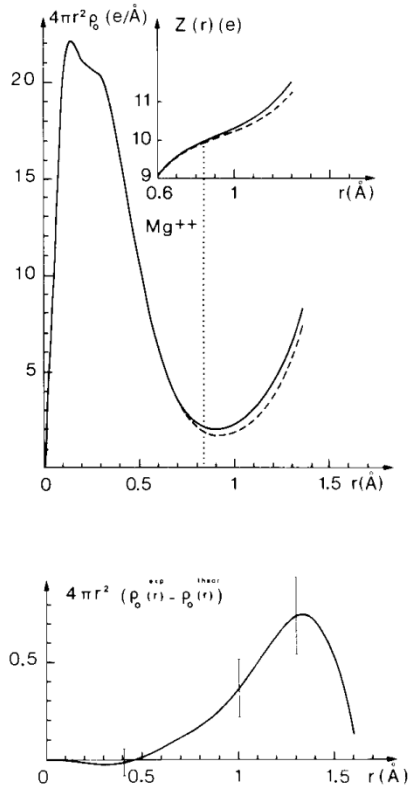

Fig. 3. Radial charge density and spherical electron count around Mg^{2+} in MgF_2. —— Experimental curve; --- theoretical curve.

$$f_{lmp}(S;\mathbf{r}_0,R) = \frac{16\pi^2 R^3}{VN_{lm}} \times \sum_j F_j \mathscr{Y}_{lmp}(\theta_j,\varphi_j)\, q_l(2\pi RS,2\pi RS_j) \times \exp(-2\pi i \mathbf{S}_j.\mathbf{r}_0); \quad (6)$$

$$q_l(x,y) = \frac{xj_{l+1}(x)\,j_l(y) - yj_{l+1}(y)\,j_l(x)}{x^2 - y^2},$$

$$N_{lm} = \int_{4\pi} [\mathscr{Y}_{lm}(\theta,\varphi)]^2\, \mathrm{d}\Omega,$$

and $j_l(x)$ is the spherical Bessel function of order l. This has the advantage that the information, as well as the errors, included in each individual structure factor F_j is approximately local in the variable $S = 2\sin\theta/\lambda$, *i.e.* smeared around S_j. Thus, the origins of different features of the results are more easily controlled whether they are due to small-angle reflexions, large-angle reflexions or cut-off errors.

The radius R of the sphere is included in the series (6) as a computational parameter. It must be chosen so that the essential features of the scattering amplitudes can be understood best as the characteristics of a one-atom contribution to the charge density (Kurki-Suonio & Salmo, 1971; Kurki-Suonio, 1968).

Here the radial charge density $4\pi r^2\rho_0$ can be used as a guide. Its minimum, in the present case 0·90 Å for Mg^{2+} and 1·25 Å for F^-, can be understood to indicate the limit up to which the charge density, averaged over all directions, behaves as centered around the atomic site. These radii of best separation yield slightly overlapping spheres of nearest neighbors. In this case $r_{Mg} + r_F = 2{\cdot}15$ Å which should be compared with the nearest-neighbor distances 1·984 and 1·995 Å and $2r_F = 2{\cdot}50$ Å to be compared with the 2·575 Å of the two neighboring fluorine atoms. Model calculations have shown that this overlapping causes negligible effects on the structure factors and that the results are not sensitive to the radii (Kurki-Suonio, 1968). In order to take into account the charge distribution extending towards the interatomic 'empty space', of which most of the whole 4π solid angle still consists, slightly 'too large' radii are considered as most suitable for calculation of f_{lmp}. In the present case the values $R_{Mg} = 0{\cdot}95$, $R_F = 1{\cdot}30$ Å were used.

The resulting radial scattering amplitudes f_{lmp} up to fourth order are given in Figs. 5 and 6 for both ions. They represent the difference series (6) with the coefficient $F_o - F_c$ with the observed and calculated structure factors of Table 2, and they refer to the local coordinate axes $(x,y,z) = (1,2,3)$ as shown in Figs. 1 and 2. Table 4 lists some numerical characteristics of the spherical behavior: the radii of best separation of the ions from their surroundings (Kurki-Suonio &

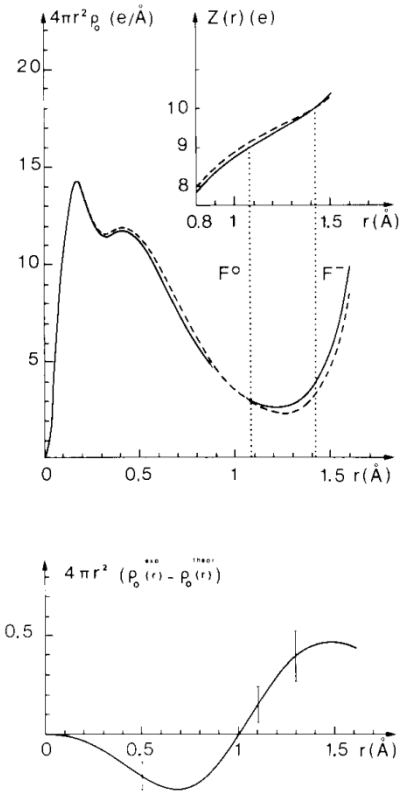

Fig. 4. Radial charge density and spherical electron count around F^- in MgF_2. ——Experimental curve; – – – theoretical curve.

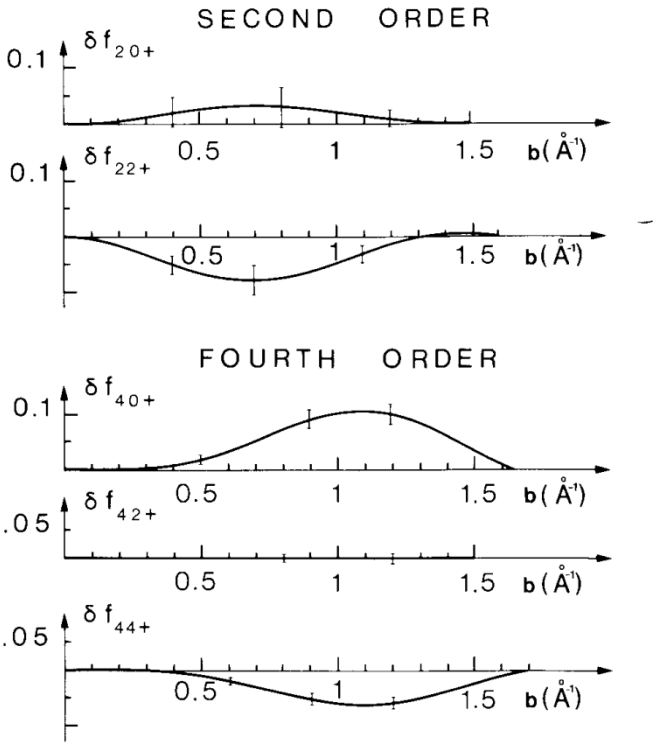

Fig. 5. Radial scattering amplitudes of the non-spherical multipole terms of Mg^{2+}.

Salmo, 1971), the minimum values of the radial charge densities and the electron counts within these radii. Table 4 lists also the electron counts responsible for the nonspherical deformations of ions within the radii of best separation as explained later in connection with the interpretation of results.

The error limits given in Table 4 refer to the standard deviations calculated from the errors $\Delta F_o/F_o$ given in Table 3.

Interpretation of the results

The spherical average radial charge density around the magnesium site, as given in Fig. 3, shows a peak in the crystal charge density which up to the radius of best separation does not essentially deviate from the corresponding peak in the theoretical density formed by the overlapping free ions. The electron count 10·10 ± 0·05 e^- of this peak indicates that it can be interpreted as a locally well defined Mg^{2+} ion in the crystal.

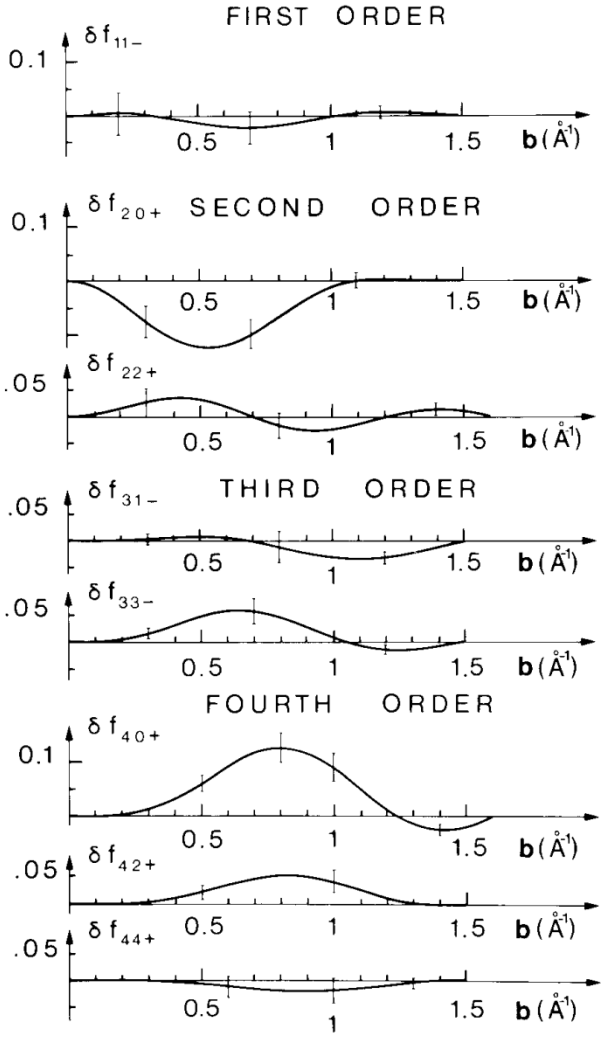

Fig. 6. Radial scattering amplitudes of the nonspherical multipole terms of F^-.

The fluorine peak shows a small monopole deformation compared to the overlapping ion model, a radial outwards transfer of about 0·1 e^-. As a whole the peak contains only 9·50 ± 0·06 electrons within the radius of best separation. This gives a picture of a local negative fluorine ion, which is much more diffuse than the positive ion, with about 0·5 electrons distributed outside the radius of the central peak. It should be noted, however, that this feature does not differ significantly from the ionic overlap model.

From the spherical behavior alone it is not possible to conclude whether the extra charge seen just beyond the peak radius of Mg^{2+} indicates increase of overlapping with the neighboring F^- ions or extension of Mg^{2+} towards interatomic space.

The radial scattering amplitudes f_{lmp} given in Figs. 5 and 6 show small but significant nonsphericities of the peaks in the crystal charge density. They represent deviations from a model where free ions are given the anisotropic harmonic vibrations deduced from the neutron data. In that context no anharmonicity was observed which could be responsible for such deviations. Therefore these are understood to be of electronic origin. If they could be attributed to some bonding effects between neighbors they would reflect the symmetry of the nearest neighborhood of each ion. The magnesium atom is at the center of a slightly distorted octahedron of neighboring fluorine atoms (Fig. 1) (*cf.* Pauling, 1928, 1980; Vidal-Valat, Vidal, Zeyen & Kurki-Suonio, 1980). This would yield an

Table 4. *Characteristics of the radial charge densities*

R = radius of best separation, $4\pi r^2 \rho_0(R)$ = minimum of the radial density, $Z_0(R)$ = electron count within the radius R.

	R (Å)		$4\pi R^2 \rho_0(R)$ (e Å^{-1})		$Z_0(R)$ (e)	
	Theoretical	Experimental	Theoretical	Experimental	Theoretical	Experimental
Mg^{2+}	0·90	0·90	1·81	2·03 ± 0·02	10	10·08 ± 0·05
F^-	1·25	1·25	2·4	2·80 ± 0·04	9·55	9·50 ± 0·06

The strengths of the nonspherical deformations (e^-) as indicated by the angular transfer of electrons from the negative lobes of $\mathcal{Y}_{lmp}(\theta, \varphi)$ to the positive ones. The significant components are marked with an asterisk.

Mg^{2+}

Z_{20+}	Z_{22+}	Z_4	Z_{42+}
0·058*	−0·008	0·084*	0·00006
±0·018	±0·022	±0·011	±0·007

F^-

Z_{11-}	Z_{20+}	Z_{22+}	Z_{31-}
−0·0039	0·085*	−0·005	0·011
±0·032	±0·030	±0·027	±0·027
Z_{33-}	Z_{40+}	Z_{42+}	Z_{44+}
−0·046*	0·0904*	0·053*	0·020
±0·022	±0·024	±0·027	±0·022

approximate local symmetry $m3m$. The axes adapted to this symmetry are obtained from the axes (1,2,3) of Fig. 1 through a 45° rotation about axis 2. Thus, in that coordinate system the multipole expansion (6) of magnesium ought to be approximately a cubic harmonic one with no second order, vanishing (42+) term and with the fixed ratio $\rho_{40+}/\rho_{44+} = 8/5$ (in terms of the harmonics normalized to maximum value 1).

The presence of significant second-order components in Fig. 5 violates this symmetry. It is found that the second order is best described as one (20+) component directed towards the axis 1 of Fig. 1. It is also easily seen that at fourth order both requirements of the approximate symmetry are definitely invalid. On the contrary, the conditions for a cubic harmonic shape of fourth order are very accurately fulfilled with respect to the lattice axes. These are related to the local axes of Fig. 1 through a 45° rotation around the 3 axis, which conserves f_{40+}, reverts the sign of f_{44+} and changes f_{22+} into f_{22-}.

On the basis of our data the electronic deformation of the magnesium peak has, thus, the form

$$d\rho_{Mg}(\mathbf{r}) = \rho_2(r)\, \mathscr{Y}_{20+}(\theta_1) + \rho_4(r)\, K_4(\theta,\varphi), \qquad (7)$$

where the polar angle θ_1 is measured from the local axis 1 and θ,φ are measured with respect to the lattice axes and K_4 is the fourth-order cubic harmonic. The corresponding radial densities $\rho_2(r)$ and $\rho_4(r)$ are shown in Fig. 7 as calculated from the series

$$\rho_{lmp}(r) = \frac{4\pi(-i)^l}{VN_{lmp}} \sum_j F_j j_l(2\pi S_j r)\, \mathscr{Y}_{lmp}(\theta_j,\varphi_j) \times \exp(-2\pi i \mathbf{S}_j.\mathbf{r}_0) \qquad (8)$$

with the notation of (6) and the coefficients $F_o - F_c$. The deviations from this form are given by the second- and fourth-order components orthogonal to (7), which turn out to be at most of the order of one quarter of the error bars shown.

It should be noted that in addition to (7) there is a dynamic nonsphericity owing to the anisotropic thermal motion subtracted from the data with the theoretical model. In principle it gives rise to all components $(2\lambda,2\mu,+)$ in the site-symmetry-adapted local coordinate system. However, only the second order is significant and is shown for comparison in Figs. 7 and 8. The different nature of the dynamic and electronic deformation is clearly visible.

It is remarkable that both components of (7) transfer charge away from the bonding directions. The second-order component carries charge from the (2,3) plane towards the axis 1, a total of $Z_2 = 0{\cdot}058 \pm 0{\cdot}019$ e$^-$ within the sphere of best separation, reducing, thus, most effectively the density between the nearest neighbors.

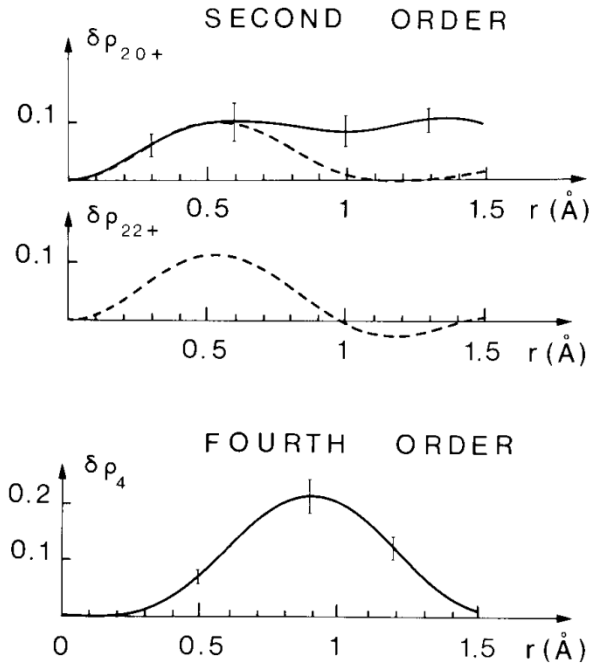

Fig. 7. Radial charge densities of the significant nonspherical multipole components of Mg^{2+}. ——Electronic deformation; – – – dynamic deformation.

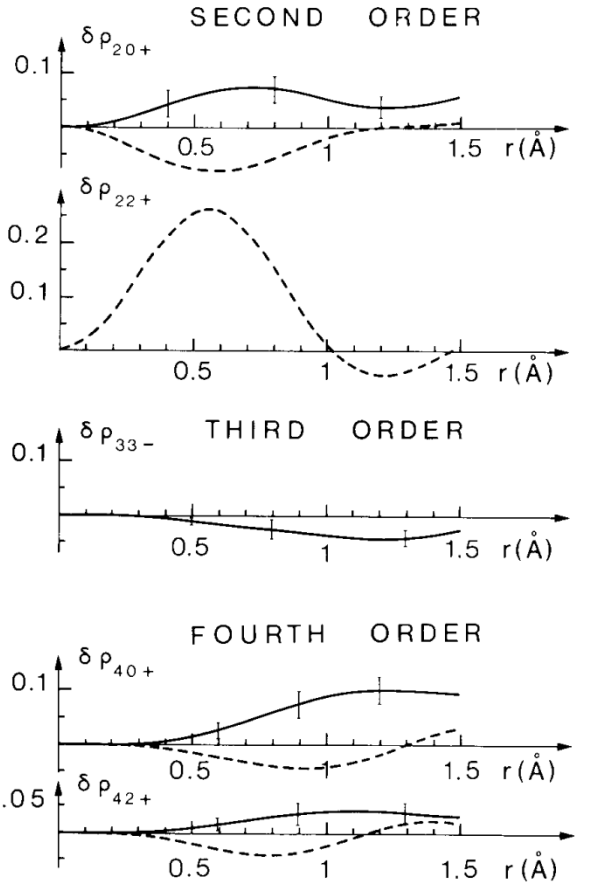

Fig. 8. Radial charge densities of the significant nonspherical multipole components of F^-. —— Electronic deformation; – – – dynamic deformation.

The cubic fourth-order component, which dominates the deformation, makes the Mg^{2+} deformation reflect the lattice symmetry rather than the approximate symmetry of the nearest neighborhood. It has maxima in the direction of crystal axes and eight minima, one in the middle of each octant of the lattice coordinate system. Four of the minima point in directions very close to the second neighbors, thus reducing the density in these 'bonds'. There are, however, four other minima in directions in the 'empty space'. The term corresponds to a total angular charge transfer of $Z_4 = 0{\cdot}084 \pm 0{\cdot}011$ e$^-$ from the minima to the maxima within the radius of best separation. Altogether, the deformation (7) can be visualized as a slightly octahedral shape of the Mg^{2+} ion with a small elongation along the local 1 axis. To make the picture more concrete, Fig. 9 shows the resulting charge density $\rho_0(r) + d\rho_{Mg}(\mathbf{r})$ along lines through the Mg site in the most important directions compared to the spherical average $\rho_0(r)$. In these curves the effect of the dynamic deformation is included.

The neighbors of the fluorine ion lie in the (2,3) plane of the local coordinate system. The Mg^{2+} ion in the negative 2 axis direction is the closest one, with the distance 1·984 Å. Two Mg^{2+} ions at an angle $\alpha = 49.77°$ from the axis 2 and a distance 1·994 Å are almost equally close. The nearest fluorine lies on the positive z axis at a distance of 2·576 Å. If the Mg neighbors alone are considered, the situation is close to the symmetry $\bar{6}m2$ with the local axis 1 as the $\bar{6}$ axis. The presence of this symmetry is easy to control by a check calculation of the multipole components in the coordinate system $(x,y,z) = (2,3,1)$, where the full site symmetry allows $(lmp) = (l,\ l-2j,\ +)$ and the $\bar{6}m2$ symmetry would destroy all except those with $m = 3\mu$. However, on the contrary, 22+ and 44+ turn out to be the largest terms.

To take into account the first fluorine neighbor a check calculation was made in terms of a 'bond deformation model'. The deformation was assumed to consist of 'bond contributions' $\Delta_i\rho = \sum d_l^{(i)}(r)\ \mathscr{Y}_{l0+}(\theta_i)$ with cylindrical symmetry with respect to the ith 'bond' direction. If the radial bond contributions $d^{(i)}(r)$ are equal for the three Mg neighbors, there are two functions d_l^{Mg} and d_l^F to be solved from $\rho_{lmp}(r)$ in each order l by a straightforward algebra of spherical harmonics. It is very clear, however, that the three components of fourth order do not allow this interpretation. Moreover, it would be expected that the bond contributions in each order would consistently reflect the strength ratio and the difference in nature of the 'bonds'. Also, this expectation of the model fails completely. It can, thus, be stated that the fluorine ion definitely reflects the crystal symmetry rather than the local symmetry of the nearest neighborhood.

According to the results presented in Fig. 6 the electronic deformation of the fluorine peak can be represented as

$$d\rho_F(\mathbf{r}) = \rho_{20+}(r)\ \mathscr{Y}_{20+}(\theta) + \rho_{33-}(r)\ \mathscr{Y}_{33-}(\theta,\varphi) + \rho_{40+}(r)[\mathscr{Y}_{40+}(\theta) + \tfrac{1}{2}\mathscr{Y}_{42+}(\theta,\varphi)], \quad (9)$$

omitting the clearly insignificant components. The radial densities ρ_{lmp} of (9) are given in Fig. 8 as calculated from the series (8).

The dominant feature of this deformation is the excess of charge in the crystal z-axis direction favored by both the major components 20+ and 40+. Differences between directions in the xy plane are less significant. However, both 33− and 42+ add to the

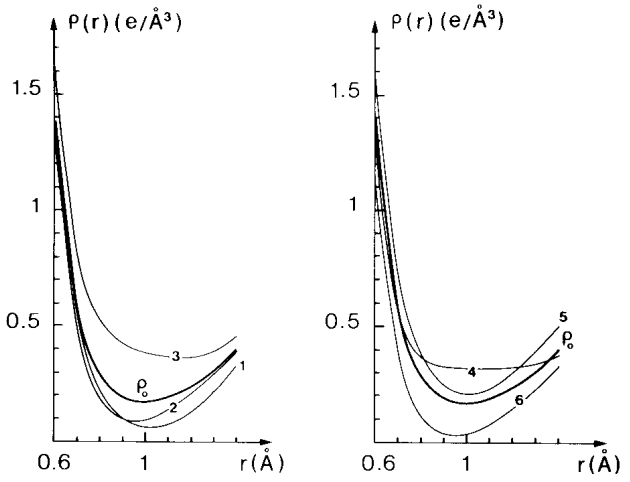

Fig. 9. Charge density obtained by multipole expansion centered at the Mg^{2+} site including the observed significant deformation components of Mg^{2+} in different directions compared to the spherical radial density $\rho_0(\mathbf{r})$. 1 Towards the first F^- neighbor; 2 towards the second F^- neighbor; 3 direction of crystal x (or y) axis; 4 direction of crystal z axis; 5 perpendicular to line 1 in the xy plane; 6 towards the minimum in 'empty' space.

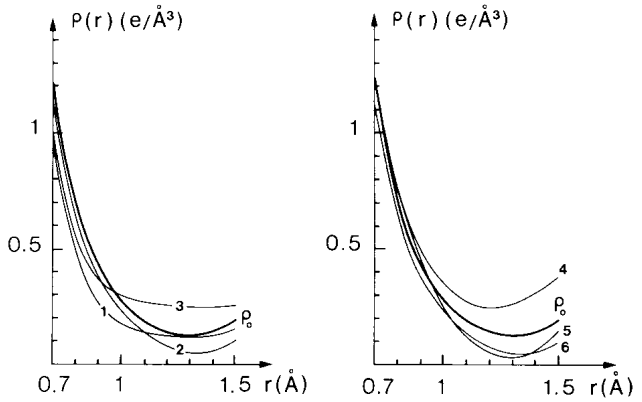

Fig. 10. Charge density obtained by multipole expansion centered at the F^- site including the observed significant deformation components of F^- in different directions compared to the spherical radial density $\rho_0(\mathbf{r})$. 1 Towards the first Mg^{2+} neighbor; 2 towards the second Mg^{2+} neighbor; 3 towards the first F^- neighbor; 4 direction of crystal z axis; 5 perpendicular to the direction 1 in the xy plane; 6 'empty' space θ_1 from z.

density on the local axis 2, *i.e.* between the two fluorine atoms, while they cancel each other on the negative 2 axis, *i.e.* in the shortest Mg–F 'bond' direction.

The relative importance of the different terms is shown by the electron counts under the positive lobes of the relevant harmonics, *i.e.* the number of redistributed electrons within the peak radius, Table 4.

The dynamic deformation due to the anisotropy of the thermal motion is not included in (9). It is shown separately for comparison in the same figures. Because the anisotropy is so large, there is now also a visible effect for fourth order.

Fig. 10 shows, for visualization of the deformation, the resulting charge density $\rho_0(r) + d\rho_F(\mathbf{r})$ along some lines through the fluorine site including the dynamic nonsphericity.

Discussion

Experimental reliability

The reliability of the observed features from the experimental point of view still needs careful consideration. The error bars and limits given in our paper so far refer only to the values of ΔF given in Table 3 and do not include any estimates of systematic errors. Most of the sources of systematic errors considered possible mainly affect the spherical behavior. So do, for example, the uncertainties in scale, isotropic extinction correction, absorption, thermal diffuse scattering and the uncertainties of the temperature factors. So the conclusions on the spherical behavior are subject to several uncertainties which are difficult to estimate.

Macroscopic bulk effects are more likely to have an effect of similar type on the different atoms. Therefore, the differences between Mg^{2+} and F^- in the nature of their deviations from the theoretical model can be considered more reliable.

The same holds true for anisotropic external sources of error. Thus, it seems difficult to think of an external reason causing such very different types of deformation as observed in magnesium and fluorine; the most likely reason to cause artefacts of this kind would be single errors in some structure factors. Therefore, special attention was paid to the reflections 110, 220, 002 and 111, which were most influenced by the extinction. Their contributions to the results obtained were checked. It was found that the fourth-order components were entirely insensitive to them. The second-order components in fluorine depend on these reflections in a way that would affect the X-ray values of the thermal anisotropies. They also have an effect on the spherical components of both ions. Moreover, changes of their values were observed to introduce a dipole component corresponding to a change in the 'X-ray value' of the position parameter or a dipole moment of fluorine.

These findings are understood to indicate that no very large single uncertainties are present in the structure factors. This opinion is further supported by the observation made from Figs. 9 and 10 that no negative values are obtained for the charge density in the neighborhood of the density peaks, which according to a general experience are very likely to occur in the presence of errors.

The additional uncertainty in the nonspherical components concerns mostly the anisotropy of the Debye–Waller factors and, hence, the division of deformations into static and dynamic components. This affects mainly the second-order. On the other hand, it must be emphasized that there is now a good agreement between the values of the Debye–Waller factors obtained by neutron diffraction, X-ray diffraction and lattice dynamical calculation (Vidal-Valat *et al.*, 1979).

Comparison with other charge density studies

Next, the results should be compared with those obtained in the case of other ionic crystals in general and particularly with CaF_2 (Ruuskanen & Kurki-Suonio, 1973) and other fluorides (Kurki-Suonio, 1971; Kurki-Suonio & Salmo, 1971) and MgO (Vidal-Valat, Vidal & Kurki-Suonio, 1978). The relationship of MgF_2 to CaF_2, which has a different structure, can be compared to the corresponding difference between MgO and CaO (Vidal-Valat, Vidal & Kurki-Suonio, 1978).

The general behavior of the spherical radial densities, as shown in Figs. 3 and 4, is similar to that of the other ionic crystals. Well defined narrow minima separate the main parts of the ions from their surroundings. This, together with the electron counts of the peaks justifies a characterization of the crystal charge density as that of a typical ionic crystal. The magnesium peak corresponds to a locally well defined Mg^{2+} ion. The fluorine peak is deficient by 0·50 e^- and presents a F^- ion of a more diffuse nature, the rest of the charge being distributed outside the spherical region considered.

In CaF_2 the fluorine was stated to be slightly 'enlarged', *i.e.* to have a monopole deformation of the same nature as shown in Fig. 4. According to the electron count, the ion was only about 0·2 e^- deficient; the fluorine ion F^- seems to be less diffuse in fluorite while the same deficiency was found in the Ca^{2+} peak. The difference in the minimum value of radial density 2·80 e $Å^{-1}$ in MgF_2 and 1·8 e $Å^{-1}$ in CaF_2 at about the same radius reflects probably the same difference in the crystals. However, the nonsphericity of F^- in MgF_2 effectively decreases the density between nearest neighbors from that indicated by the spherical behavior, *cf.* Fig. 10. This indicates that the difference is due to the geometry of the crystal rather than the degree of compactness of fluorine. For lower site

symmetry (*mm*2) and highly anisotropic thermal motion in MgF_2 the spherical description gives a more smeared-out picture of fluorine than in the case of high site symmetry ($\bar{4}3m$) and spherical motion of F^- in CaF_2. The comparable values for electron count deficiency and minimum radial density 0·25 e^-, 2·0 $e\,Å^{-1}$ and 0·3 e^-, 1·8 $e\,Å^{-1}$ for fluorine in NaF and LiF, respectively, (Kurki-Suonio & Salmo, 1971; Kurki-Suonio, 1971) suggest that fluorine as a crystal atom has some rather well defined ionic state occurring in ionic crystals.

According to the data of Sanger (1969) (*cf.* Vidal-Valat, Vidal & Kurki-Suonio, 1978), magnesium in MgO differs considerably from the magnesium ion in MgF_2. The spherical behavior shows a considerable charge excess in the outer region so that the peak corresponds with Mg^+ rather than Mg^{2+} and the radius of best separation increases to the large value of 1·03 Å compared to the present 0·9 Å. In spite of the larger radius the nonsphericity is minute, if not negligible, as compared to the present case.

In both ions of MgF_2, the nonsphericities reflect clearly the crystal symmetry and not the symmetry of the near surroundings. The ions have a shape which clearly improves their separability from their surroundings compared with the picture given by the spherical radial densities and with the overlapping free-ion model. Both features emphasize the ionic nature of the crystals. The latter property of the deformations has been stated earlier in some ionic crystals (*cf.* Vahvaselkä & Kurki-Suonio, 1975). One can, however, note that according to the radial difference density in Fig. 3 there seems to be a small excess of charge attached to the Mg^{2+} ion just beyond the peak radius. Taking into account the shape of the nonsphericities, this must be due to bulging of charge density towards the interatomic empty regions rather than to the neighboring fluorine atoms.

The experimental charge density study of Niederauer & Göttlicher (1970) is partially in contradiction with ours. The electron counts agree. The results concerning the charge densities between the nearest neighbors are essentially different. While they find some 'covalent bonding density' between both the first- and the second-closest Mg–F neighbors, the nonsphericities deduced from our data reduce the charge density in both 'bonds' to considerably lower values (0·6 to 1·0 $e\,Å^{-3}$), without significant difference between the first and second neighbors, in accordance with a completely ionic character for the bond. The difference between the two bonds in Fig. 10 is almost entirely due to the dynamic anisotropy. Compared to these values, the density between the two closest fluorine atoms takes a larger value, 0·25 $e\,Å^{-3}$, a small part of which comes from the dynamic anisotropy. This is not really contradictory to the value of 1·8 $e\,Å^{-3}$ found by Niederauer & Göttlicher (1970). The extension of the charge density, from Mg^{2+}, towards all crystal axis directions and from F^- to the *z*-axis direction, differs, however, decisively from the findings of Niederauer & Göttlicher. On the other hand, a multipole analysis of the data given in the paper of Niederauer & Göttlicher yields exactly spherical results for the ionic peaks without any nonsphericities whatsoever, which questions the meaning of the comparison of their statements on charge density with ours. Also, they did not find any anisotropy of the thermal motion, which is not consistently confirmed by both neutron and X-ray diffraction as well as lattice dynamical calculations (Vidal-Valat, Vidal, Zeyen & Kurki-Suonio, 1979).

Ionicity, deformability and polarizability

While our results as such may be qualitatively understandable and are in accordance with the results of some other comparable studies, they seem to be in contradiction with quantitative theoretical considerations.

The lattice dynamical calculations by Almairac & Benoit (1974) based on experimental phonon spectra yield effective charges corresponding to a high degree of ionicity in accordance with the charge density. However, they indicate a negligible polarizability of the Mg^{2+} ion compared to fluorine. Also, the extensive studies by Tessman, Kahn & Schockley (1953) and Pauling (1927) of ionic polarizabilities in cubic crystals yields for Mg^{2+} a value 0·1 times that of F^- based on experimental optical results.

The valence-band calculations of Jouanin & Gout (1972) assume complete ionicity. The large difference in energies of the F^- and Mg^{2+} orbital bands indicates very small deformability of Mg^{2+} compared to F^-, in accordance with the lattice dynamical conclusions. Our results, on the contrary, show non-spherical deformations of electronic origin of about the same order of magnitude for both ions. Also, it seems unpredictable that the dominant components are of fourth order and that the first order or dipole deformation of F^- is zero when higher orders are not. This last statement indicates a zero dipole moment for fluorine, *cf.* Bertaut (1979). To understand this discrepancy one should pay attention to the difference in the nature of the descriptions. The charge density gives a strictly local view of the situation. The atoms appear there as local entities, peaks of the crystal charge density. There is therefore a subtle difference in the concept of atoms in the different treatments. The free-atom wave functions, like the free-atom charge densities, have necessarily no relevance from the point of view of crystal atoms as local structural entities. From the point of view of the charge density we can refer to the well known fact that there is no essential difference between the total charge

densities of the free atom overlapping models, say, K^0Br^0 and K^+Br^-. Both display local peaks with electron counts corresponding most closely to an ionic crystal (Kurki-Suonio & Salmo, 1971; Kurki-Suonio, 1971). To see the real relationship of theory with our results a theoretical charge density calculation would be necessary.

In view of the overlap integrals given by Jouanin & Gout (1972), which decrease slowly with the increase in the distance of neighbors, it is understandable that the electronic nonsphericities of the 'charge density atoms' follow the total crystal symmetry rather than the symmetry of the neighbors, particularly when no covalent bonding occurs. The small polarizability of Mg^{2+} also does not necessarily indicate more than a small deformability of the local atom from its natural shape, whatever it is in the crystal. We can, thus, understand that it is the compactness of the Mg^{2+} peak compared to the diffuse nature of the F^- peak that reflects the difference in polarizability, rather than the nonsphericities of the peaks. We can also note that the optical and spectroscopic results and the theoretical values refer only to dipole moments.

These considerations seem to indicate that the origin of the deformations, if they are real, must be traced back to some wave-function algebra including the necessary orthogonalization of single Fermion wave functions and the translation into the local charge-density description of crystal atoms, which must be considered as zeroth-order effects, rather than to any perturbations caused by the dynamic interactions.

APPENDIX

Calculation of the atomic mean-square displacements

Let

$$u_{\alpha\beta}(J) = \langle\langle u_\alpha(J).u_\beta(J)\rangle\rangle_{\text{Av}},$$

where $J = 1, 2, \ldots, g$ labels the g atoms of the unit cell, $\alpha = 1, 2, 3$, $\beta = 1, 2, 3$ refer to Cartesian axes and the brackets to the thermal average.

The thermal average can be calculated as a sum in reciprocal space:

$$u_{\alpha\beta}(J) = \sum_{\mathbf{K},S} \frac{\hbar}{NM_J} \frac{1}{\omega(\mathbf{K},S)} \text{Re}[V_{J\alpha}(\mathbf{K},S)\, V^*_{J\beta}(\mathbf{K},S)] \times \{[\exp(\hbar\omega/K_b T) - 1]^{-1} + \tfrac{1}{2}\},$$

where M_J is the mass of atom J, $V_{J\alpha}(\mathbf{K},S)$ are the components of the polarization vectors obeying the orthogonality relations

$$\sum V_{J\alpha}(\mathbf{K},S)\, V^*_{J\alpha}(\mathbf{K},S') = \delta(S,S')$$

and $S = 1, 2, \ldots, 3g$ labels the different lattice modes of wave vector $\mathbf{K}$. N is the number of cells in the crystal. The frequencies and polarization vectors necessary to calculate the reciprocal-space sum have already been determined by Almairac (1975) with a shell model fitted to inelastic neutron scattering results. 126 different values of $\mathbf{K}$ were taken in the reduced Brillouin zone (which is 1/16 of the total one) giving 126×18 frequencies and polarization vectors (see Fig. 11). This process, however, cannot account for the acoustic vibrations near the center of the Brillouin zone, because of the vanishing frequencies of these modes. We therefore exclude them from the sum, and give a separate evaluation of their contribution to u.

It is well known that the polarization vectors for acoustic modes 'a' are of the form

$$V_{J\alpha}(\mathbf{K},S) = \sqrt{\frac{M_J}{M}}\, t_{\alpha,a}(\Omega)$$

($M = \sum_J M_J$) and the frequencies

$$\omega(\mathbf{K},S) = C_a(\Omega).|\mathbf{K}|.$$

$C_a(\Omega)$ is one of the three velocities of sound in the direction Ω, $t_{\alpha,a}(\Omega)$ are the corresponding components of the polarization vectors which are now independent of the atom. Both are easily deduced, for each direction Ω, from the elastic constants.

With these new parameters, the contribution of the acoustic modes in a volume V located in the center of the Brillouin zone is

$$\frac{\hbar v_m}{(2\pi)^3} \sum_a \int_V \frac{\mathrm{d}v}{|\mathbf{K}|\, C_a(\Omega)}\, t_{\alpha,a}(\Omega) \times t^*_{\beta,\alpha}(\Omega)\{[\exp(\hbar\omega/K_b T) - 1]^{-1} + \tfrac{1}{2}\}$$

where v_m is the cell volume. The integral is evaluated in polar coordinates:

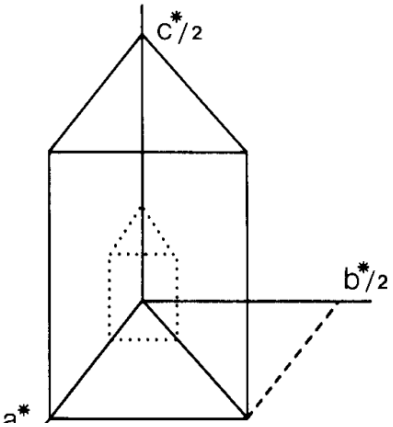

$$\frac{\hbar v_m}{(2\pi)^3}\sum_a \int \frac{d\Omega}{C_a(\Omega)}\, t_{\alpha,a}(\Omega)\, t^*_{\beta,a}(\Omega) \times \int_0^{K_m(\Omega)} K dK \left(\{\exp[\hbar C_a(\Omega)\, K/K_b\, T] - 1\}^{-1} + \tfrac{1}{2}\right).$$

The integral over K may be written

$$[K_m(\Omega)]^2\, \varphi\left[\frac{\hbar C_a(\Omega)\, K_m(\Omega)}{K_b\, T}\right],$$

where φ is the function

$$\varphi(x) = \frac{1}{x^2}\int_0^x \left(\frac{1}{e^u - 1} + \frac{1}{2}\right) u\, du$$

and the acoustic contribution from the volume V is

$$\frac{\hbar v_m}{(2\pi)^3}\sum_a \int \frac{[K_m(\Omega)]^2}{C_a(\Omega)}\, t_{\alpha,a}(\Omega) t^*_{\beta,a}(\Omega) \times \varphi\left[\frac{\hbar C_a(\Omega)\, K_m(\Omega)}{K_b\, T}\right] d\Omega.$$

For numerical calculations, the volume V was chosen as similar to the reduced Brillouin zone in the linear ratio of 0·3, *cf.* Fig. 11. In this volume the Ω integration was replaced by a finite sum over 26 different directions.

The elastic constants are taken from the work of Aleksandrov, Shabanova & Zinenko (1969). The calculations give for Mg^{2+} $u_{11} = u_{22} = 0{\cdot}0066$, $u_{33} = 0{\cdot}0046$ and $u_{12} = 0{\cdot}0006$ Å^2, and for F^- $u_{11} = u_{22} = 0{\cdot}0065$, $u_{33} = 0{\cdot}0068$ and $u_{12} = -0{\cdot}0034$ Å^2.

References

ALEKSANDROV, K. S., SHABANOVA, L. A. & ZINENKO, V. L. (1969). *Phys. Status Solidi*, **33**, 1–3.

ALMAIRAC, R. (1975). Thesis, Montpellier.

ALMAIRAC, R. & BENOIT, C. (1974). *J. Phys. C*, **7**, 2614–2648.

BARKER, A. S. (1964). *Phys. Rev. A*, **136**, 1290.

BECKER, P. J. & COPPENS, P. (1975). *Acta Cryst.* A**31**, 417–425.

BERTAUT, E. F. (1979). *J. Phys. (Paris)*, **39**, 1331–1348.

BUSING, W. R. & LEVY, H. A. (1957). *Acta Cryst.* **10**, 180–182.

CROMER, D. T. & LIBERMAN, D. (1970). *J. Chem. Phys.* **53**, 1891–1898.

GOUT, C., LAHAYE, B. & PERRIER, P. C. R. (1967). *C.R. Acad. Sci. Ser. B*, **265**, 1460–1462.

JOUANIN, C., ALBERT, J. P. & GOUT, C. (1976). *J. Phys. (Paris)*, **37**, 595–602.

JOUANIN, C. & GOUT, C. (1972). *J. Phys. C*, **5**, 1945–1952.

KURKI-SUONIO, K. (1968). *Acta Cryst.* A**24**, 379–390.

KURKI-SUONIO, K. (1971). Italian Crystallographic Association Meeting, Bari, Italy.

KURKI-SUONIO, K. (1977). *Isr. J. Chem.* **16**, 115–123, 132–136.

KURKI-SUONIO, K., MERISALO, M. & PELTONEN, H. (1979). *Phys. Scr.* **19**, 57–63.

KURKI-SUONIO, K. & SALMO, P. (1971). *Ann. Acad. Sci. Fenn. Ser. A*6, p. 369.

MATSUMOTO, M., URABE, K. & KANAMORI, H. (1978). *Indian J. Pure Appl. Phys.* **16**, 263–267.

MISHRA, K. C., PADHY, B. & MOHANTY, B. S. (1977). *Indian J. Pure Appl. Phys.* **15**, 405–408.

NIEDERAUER, K. & GÖTTLICHER, S. (1970). *Z. Angew. Phys.* pp. 16–21.

PAULING, L. (1927). *Proc. R. Soc. London Ser. A*, **114**, 181–211.

PAULING, L. (1928). *Z. Kristallogr.* **67**, 377–404.

PAULING, L. (1980). *Acta Cryst.* B**36**, 761–762.

POOLE, R. T., SZAJMAN, J., LECKEY, R. C. G., JENKIN, J. G. & LIESEGANG, J. (1975). *Phys. Rev. B*, **12**, 5872–5877.

PORTO, S. P. S., FLEURY, P. A. & DAMEN, T. C. (1967). *Phys. Rev.* **154**, 522.

RABE, P., SONNTAG, B., SAGAWA, T. & HAENSEL, R. (1972). *Phys. Status Solidi B*, **50**, 559–563.

RUUSKANEN, A. & KURKI-SUONIO, K. (1973). *J. Phys. Soc. Jpn*, **34**, 715–719.

SANGER, P. L. (1969). *Acta Cryst.* A**25**, 694–702.

TESSMAN, J., KAHN, A. & SCHOCKLEY, W. (1953). *Phys. Rev.* **92**, 890–894.

THOMAS, J., STEPHAN, G., LEMONNIER, J. C., NISAR, M. & ROBIN, S. (1973). *Phys. Status Solidi B*, **56**, 163–170.

VAHVASELKÄ, A. & KURKI-SUONIO, K. (1975). *Phys. Fenn.* **10**, 87–99.

VENGHAUS, H. (1971). *Opt. Commun.* **2**, 447–449.

VIDAL-VALAT, G., VIDAL, J. P. & KURKI-SUONIO, K. (1975). Report Series in Physics, No. 107, Helsinki.

VIDAL-VALAT, G., VIDAL, J. P. & KURKI-SUONIO, K. (1978). *Acta Cryst.* A**34**, 594–602.

VIDAL-VALAT, G., VIDAL, J. P., ZEYEN, C. & KURKI-SUONIO, K. (1979). *Acta Cryst.* B**35**, 1584–1590.

VIDAL-VALAT, G., VIDAL, J. P., ZEYEN, C. & KURKI-SUONIO, K. (1980). *Acta Cryst.* B**36**, 2857.

WILLIAMS, M. W., MACRAE, R. A. & ARAKAWA, E. T. (1967). *J. Appl. Phys.* **38**, 1701–1705.